Triple-layer configuration for stable high-speed lubricated pipeline transport

Parisa Sarmadi,[1] Sarah Hormozi,[2] and Ian A. Frigaard[1,3,*]

[1]*Department of Mechanical Engineering, University of British Columbia, 2054-6250 Applied Science Lane, Vancouver, British Columbia, Canada V6T 1Z4*

[2]*Department of Mechanical Engineering, Russ College of Engineering and Technology, Ohio University, 251 Stocker Center, Athens, Ohio 45701-2979, USA*

[3]*Department of Mathematics, University of British Columbia, 1984 Mathematics Road, Vancouver, British Columbia, Canada V6T 1Z2*

(Received 5 November 2016; published 28 April 2017)

Lubricated transport of heavy viscous oils is a popular technology in the pipelining industry, where pumping pressures can be reduced significantly by concentrating the strain rate in a lubricating layer. However, the interface between the lubricating layer and heavy oil is vulnerable to any perturbations in the system as well as transients due to start up, shut down, temperature change, etc. We present a method in which we purposefully position an unyielded skin of a viscoplastic fluid between the oil and the lubricating fluid. The objective is to reduce the frictional pressure gradient while avoiding interfacial instability. We study this methodology in both concentric and eccentric configurations and show its feasibility for a wide range of geometric and flow parameters found in oil pipelining. The eccentric configuration benefits the transport process via generating lift forces to balance the density differences among the layers. We use classical lubrication theory to estimate the leading order pressure distribution in the lubricating layer and calculate the net force on the skin. We explore the effects of skin shape, viscosity ratio, and geometry on the pressure drop, the flow rates of skin and lubricant fluids, and the net force on the skin. We show that the viscosity ratio and the radius of the core fluid are the main parameters that control the pressure drop and consumptions of outer fluids, respectively. The shape of the skin and the eccentricity mainly affect the lubrication pressure. These predictions are essential in designing a stable transport process. Finally, we estimate the yield stress required in order that the skin remain unyielded and ensure interfacial stability.

DOI: 10.1103/PhysRevFluids.2.044302

I. INTRODUCTION

The past 20 years have seen a progressive shift towards heavy-oil production as easier light oils are progressively consumed. Due to significantly increased viscosities, the transportation of heavy oil in pipelines is an increasingly important problem. Coupled with increased production of *waxy* crude oils, which can precipitate gel-like (viscosifying) structures, the management of frictional pressure losses and ensuring continued flow (flow assurance) have become important areas of pipeline engineering, operationally and in design stages. This has led to a revival of interest in core-annular flows, originally proposed 50 years ago as a method of reducing friction [1]. Conceptually, the lower viscosity of the lubricating fluid reduces friction. However, the viscosity mismatch at the liquid-liquid interface and significant buoyancy forces between fluids can combine to induce interfacial instabilities at even modest flow rates, which can compromise transport effectiveness; see, e.g., Refs. [2–5].

The objective of this paper is to present a method of crude oil transportation via core-annular flow, and establish its feasibility for some practical classes of pipelining flows. A triple-layer structure is considered in which a viscoplastic fluid is inserted between transported and lubricating fluid, acting

*Corresponding author: frigaard@math.ubc.ca

as a *skin* layer. This is combined with the usual low viscosity Newtonian fluid along the pipe wall, to lubricate transport, and heavy viscous oil is the core fluid.

The idea of the triple-layer structure originates from viscoplastic lubrication (VPL) flows, as studied by Moyers-Gonzalez *et al.* [6] and Hormozi *et al.* [7]. In these flows the yield stress is used to eliminate the possibility of interfacial instability growth, by remaining rigid. Frigaard [8] studied the linear stability of a multilayer plane Poiseuille flow of two Bingham fluids, exposing the role of the yield stress in freezing the interface. Moyers-Gonzalez *et al.* [6] extended the analysis to viscoplastically lubricated viscous core-annular pipe flows and derived nonlinear stability bounds. Huen *et al.* [9] demonstrated experimentally that these flows can be stably established. The range of applications was extended by Hormozi and co-workers [7,10,11]. When the interface is formed by two yielded fluids, the stability is lost and interfaces are vulnerable to the usual range of linear instabilities, as explored by Sahu *et al.* [12,13].

The second component contributing to the triple-layer structure comes from our understanding of core-annular flows. Ooms, Bai, and others initiated the study of how shaped eccentrically positioned core-annular interfaces generate differential lubrication pressures around the core; see, e.g., Refs. [14–16]. The generation of lubrication pressures requires that the interface profile varies in the streamwise direction, whereas the eccentricity of the core focuses the differential pressure around the core, according to the lubricating fluid layer thickness. The differential pressure can be used to balance the density mismatch between the fluids (the oil usually being lighter). More recently, Ooms and co-workers [17,18] have studied eccentric core-annular flow of a very-viscous core, i.e., a solid, analytically and semianalytically using hydrodynamic lubrication theory.

Our study combines these two component ideas. We proceed in a number of steps: (i) We consider the lubricating layer to be relatively thin, so that even for significant Reynolds numbers the inertial terms are negligible at leading order. We then use classical lubrication theory to estimate the leading order pressure distribution in the lubricating fluid layer. (ii) By integrating over the lubricating fluid layer we calculate the net force on the skin and core fluids. (iii) By adjusting the shape of the skin we may make the net force positive or negative. By adjusting the eccentricity of the layer we may increase or decrease the net force. (iv) By balancing with the buoyancy force acting on the skin and core fluids, we establish the equilibrium position of the transported core. (v) Finally, on calculating the stresses within the lubrication layer we can estimate the yield stress required to keep the skin rigid.

This leaves one final piece in the puzzle, namely, how can we form shapes in the viscoplastic skin in such a way that they remain rigid when formed, what fluids should be used for the skin, and can this be done continuously as the fluids are pumped and pipelined. This part of the process concept is not fully researched, but we believe there is sufficient reason to believe in its feasibility. We envisage the process sequentially in three parts [Fig. 1(a)]: (a) a concentric inflow manifold in which the multilayer flow is constructed; (b) a transient length, on leaving the manifold, within which the core fluid *floats* to its steady eccentric position; and (c) steady, fully developed flow along a pipeline. This paper is directed at the mechanics of (c).

Regarding (a), concentric manifolds have been used to establish multilayer flows for many years. Specific to flows in which a yield stress fluid is used, Ref. [9] demonstrated that stable flows of given design radii can be routinely established. Figure 1(b) illustrates a simple extension of a two-layer flow design, allowing the controlled initial development of the concentric core-skin interface (essentially as in Ref. [9]), followed downstream by a region in which the shaped skin-lubricant interface can be formed. Development lengths within the initial part of the manifold have been studied in Ref. [7], so that distance to the shaping zone can be quantified.

On entering the shaping zone, the fluid at the skin-lubricant interface is yielded, whereas that at the core-skin interface is unyielded. *Sculpting* of the outer interface can therefore take place, up until the time at which the stresses relax sufficiently for the skin-lubricant interface to become unyielded. Two principal avenues are available to sculpt a given shape: (i) controlled variation in the flow rates of the lubricant (and/or skin), and (ii) mechanical variation of the aperture. The first of these is the subject of our ongoing research and we believe shows some promise.

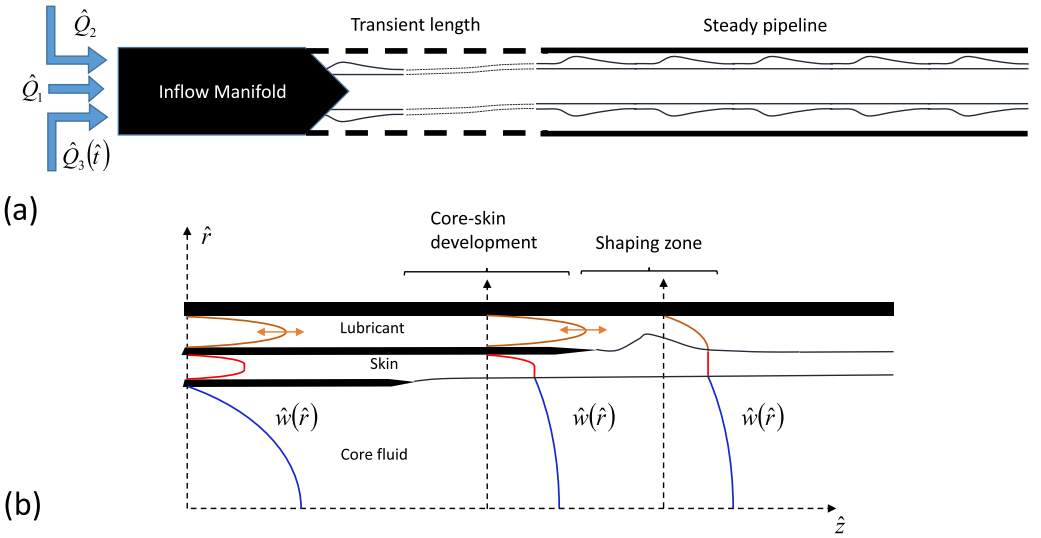

FIG. 1. (a) Conceptual zones of triple-layer flow. (b) Flow development within the inflow manifold.

In the limit of a slowly varying interface shape, the mapping from the flow rate to shape is direct. The sculpting process can also be influenced by fluid rheology, which may control interfacial deformation before the skin relaxes to a solid shape. In Ref. [19] it was observed experimentally that unstable interfacial waves would freeze into the unyielded interface as VPL flows developed. Hormozi *et al.* [20] used computational and experimental methods to show that variations in the individual flow rates of the two fluid streams allowed some degree of control over the interface shape (i.e., wavelength and amplitude). Figure 2 shows an example flow in which a diamond-shaped

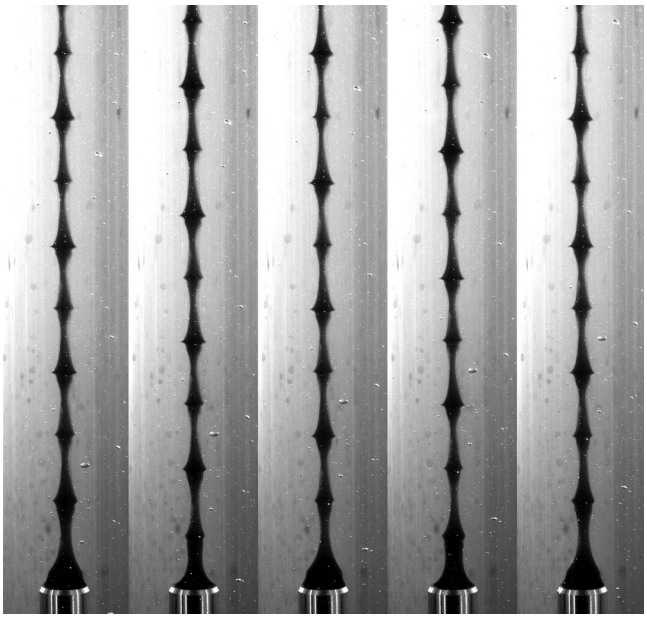

FIG. 2. Example of interface shapes sculpted near the inflow pipe and then frozen into a shaped solid interface advected downstream (for parameters and description, see Fig. 15(a) in Ref. [20]).

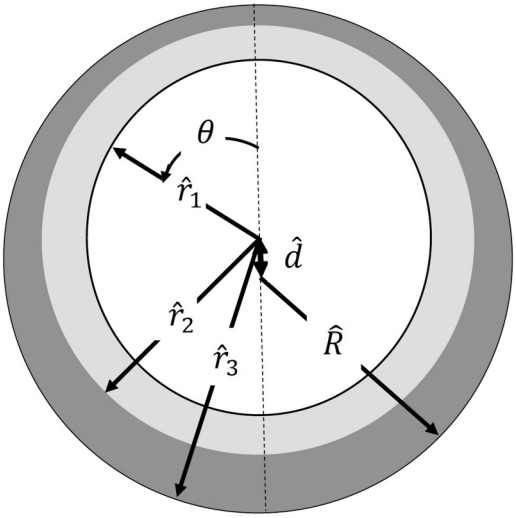

FIG. 3. Cross section of the pipe with triple-layer configuration.

interface is sculpted into the flow near the inflow pipe and then freezes into a shaped solid interface which is advected downstream. In related work, Maleki *et al.* [21] showed how liquid droplets could be encapsulated in a flowing stream of unyielded fluid.

Regarding the transient length, region (b), this is less well understood but appears to be a simpler problem, which may be estimated reasonably using methods similar to those used here. In conclusion, to some extent the mechanical feasibility of forming a stable shaped interface is already established, but the fundamental understanding of how to control the shape needs work.

Our paper starts by introducing the flow setup and notation (Sec. II) and then moves onto a concentric flow configuration that allows a semianalytical solution. Next, the eccentric case is examined for various variables, following through the steps (i)–(v) outlined above. The paper closes with a discussion of the feasibility of the proposed method for lubricated transport.

II. FLOW DESCRIPTION

As explained in Sec. I, our aim in this paper is to study core-annular configurations that allow the generation of lift via hydrodynamic lubrication, while at the same time resisting interfacial deformation via the introduction of an unyielded skin layer. Consider therefore a section of the pipe, periodic in the streamwise $\hat{z}$ direction and assumed horizontal for simplicity. The entire flow domain is denoted Ω and the three individual fluid domains by Ω_1, Ω_2, and Ω_3. Fluid 1 denotes the core fluid (viscous Newtonian heavy oil), with viscosity $\hat{\mu}^{[1]}$ and density $\hat{\rho}^{[1]}$. The skin layer is fluid 2, modeled simply as a Bingham fluid, with $\hat{\mu}^{[2]}$, $\hat{\tau}_y^{[2]}$, and $\hat{\rho}^{[2]}$ denoting its viscosity, yield stress, and density, respectively. Fluid 3 is the lubrication layer (assumed to be a low viscosity Newtonian fluid) with viscosity $\hat{\mu}^{[3]}$, and density $\hat{\rho}^{[3]}$. Figure 3 indicates schematically the positions of the three fluids, within a cross section of the pipe at fixed $\hat{z}$.

The outer radius of the skin may vary with $\hat{z}$, $\hat{r} = \hat{r}_2 = \hat{r}_{2,0} + \Delta\hat{r}_2\Phi(\hat{z})$, but the inner radius ($\hat{r} = \hat{r}_1$) is uniform; see Fig. 4. The skin fluid is assumed to have a sufficiently high yield stress that it remains rigid (unyielded). Thus, fluids 1 and 3 remain separated. In general, we might assume that the yield stress required is moderately large (estimated later) and the pipe diameter is >0.1 m, so that any surface tension effects are negligible in comparison to the other stresses.

The governing equations for the flow are the Navier-Stokes equations, in each fluid domain. The traction and velocity vectors are continuous across each interface (neglecting surface tension,

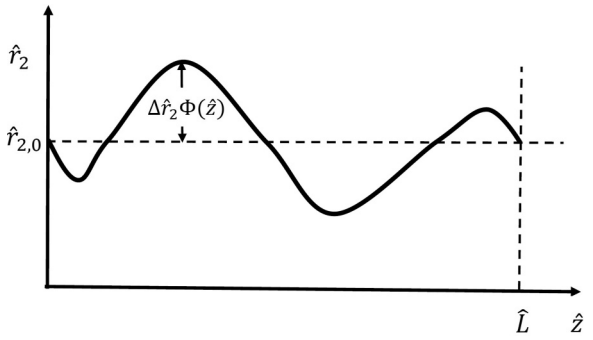

FIG. 4. Schematic of the outer radius variation of skin layer with $\hat{z}$, characterized via the mean outer radius $\hat{r}_{2,0}$ and streamwise variation $\Delta\hat{r}_2\Phi(\hat{z})$.

as argued above). The flow is periodic in $\hat{z}$ and no-slip conditions are satisfied at the pipe wall. Constitutive equations for the three fluids are

$$\hat{\tau}_{ij}^{[k]} = \hat{\mu}^{[k]}\hat{\dot{\gamma}}_{ij}, \quad k = 1,3, \tag{1}$$

$$\hat{\tau}_{ij}^{[2]} = \left[\hat{\mu}^{[2]} + \frac{\hat{\tau}_y^{[2]}}{|\hat{\dot{\gamma}}|}\right]\hat{\dot{\gamma}}_{ij} \Longleftrightarrow \hat{\tau}^{[2]} > \hat{\tau}_y^{[2]}, \tag{2}$$

$$\hat{\dot{\gamma}} = 0 \Longleftrightarrow \hat{\tau}^{[2]} \leqslant \hat{\tau}_y^{[2]}, \tag{3}$$

where

$$\hat{\dot{\gamma}}_{ij} = \frac{\partial\hat{u}_i}{\partial\hat{x}_j} + \frac{\partial\hat{u}_j}{\partial\hat{x}_i},$$

$$\hat{\dot{\gamma}} = \left[\frac{1}{2}\sum_{i,j=1}^{3}[\hat{\dot{\gamma}}_{ij}]^2\right]^{1/2}, \quad \hat{\tau}^{[2]} = \left[\frac{1}{2}\sum_{i,j=1}^{3}\left[\hat{\tau}_{ij}^{[2]}\right]^2\right]^{1/2}. \tag{4}$$

Concentric core-annular flow

We start with a brief analysis of fully developed steady concentric flows, with no buoyancy and a uniform skin layer. In order to scale the equations, we focus on transport of the core fluid, which is assumed to have a flow rate $\hat{Q}_1$. We use $\hat{Q}_1$ to define the velocity scale, $\hat{W}_0 = \hat{Q}_1/\pi\hat{R}^2$, which we see is the velocity of the heavy oil, if transported alone in the pipe. We scale all lengths with $\hat{R}$. The stress scale is $\hat{\mu}^{[3]}\hat{W}_0/(\hat{R} - \hat{r}_{2,0})$, used for both the deviatoric stresses and pressure, representing the shear stress in the lubrication layer,

$$(r,z) = \frac{(\hat{r},\hat{z})}{\hat{R}}, \quad \mathbf{u} = \frac{\hat{\mathbf{u}}}{\hat{W}_0}, \quad -G_c = \frac{\partial p}{\partial z} = \frac{\partial\hat{p}}{\partial\hat{z}}\frac{\hat{R}(\hat{R} - \hat{r}_{2,0})}{\hat{\mu}^{[3]}\hat{W}_0}, \quad \tau_{zr} = \frac{\hat{\tau}_{zr}(\hat{R} - \hat{r}_{2,0})}{\hat{\mu}^{[3]}\hat{W}_0}.$$

This leads to a problem governed by two dimensionless radii, r_1 and $r_{2,0}$, and two further dimensionless groups,

$$m = \frac{\hat{\mu}^{[3]}}{\hat{\mu}^{[1]}}, \quad B = \frac{\hat{\tau}_y^{[2]}(\hat{R} - \hat{r}_{2,0})}{\hat{\mu}^{[3]}\hat{W}_0}.$$

Here, m is the viscosity ratio and B is the Bingham number. Provided that the skin layer remains unyielded, the second viscosity ratio $\hat{\mu}^{[2]}/\hat{\mu}^{[1]}$ plays no role in the flow. Steady unidirectional flow

is governed by the z-momentum equation,

$$-G_c = \frac{1}{r}\frac{\partial}{\partial r}\left[r\tau_{zr}^{[k]}\right], \tag{5}$$

where $k = 1,2,3$ represent the three fluid layers. The shear stresses and velocities are constant at each interface; G_c is constant, representing the modified axial pressure gradient for the concentric flow. In the main case of interest, when the skin layer is completely unyielded, the axial velocity is

$$W(r) = \begin{cases} W_p\left[1 + m\frac{r_1^2 - r^2}{1 - r_{2,0}^2}\right], & 0 \leqslant r < r_1, \\ W_p, & r_1 \leqslant r < r_{2,0}, \\ W_p\frac{1-r^2}{1-r_{2,0}^2}, & r_{2,0} \leqslant r < 1, \end{cases} \tag{6}$$

where

$$W_p = \frac{G_c(1 + r_{2,0})}{4}$$

is the *plug* velocity. The pressure gradient G_c is found by ensuring a unit flow rate through Ω_1 (due to the chosen scaling),

$$G_c = \frac{8\pi}{\frac{m}{\delta}r_1^4 + 2r_1^2\pi(1 + r_{2,0})}, \tag{7}$$

where $\delta = (\hat{R} - \hat{r}_{2,0})/\pi\hat{R}$, which is the aspect ratio of the thin lubricant layer thickness to the circumferential length scale. Finally, by calculating the shear stresses we will estimate the yield stress required in order to have an unyielded skin layer,

$$B > \frac{G_c r_{2,0}}{2} = \frac{4\pi r_{2,0}}{\frac{m}{\delta}r_1^4 + 2r_1^2\pi(1 + r_{2,0})}. \tag{8}$$

In other words, for a given geometry this type of flow becomes feasible for a sufficiently large yield stress. Note also that $G_c \sim O(1)$, indicating that the viscous stress in the lubrication layer is the relevant scale, and since typically $m/\delta \ll 1$, the constraint on B is not severe, i.e.,

$$\hat{\tau}_y^{[2]} \sim \frac{\hat{\mu}^{[3]}\hat{W}_0}{\hat{R}(1 - r_{2,0})}.$$

Assuming (8) to hold, the viability of the lubrication process depends on the consumption of the skin and lubricant fluids, plus whether or not the frictional pressure has been reduced.

The scaled flow rates (Q_2, Q_3) are

$$Q_2 = 2\int_{r_1}^{r_{2,0}} W(r)rdr = \left[r_{2,0}^2 - r_1^2\right]W_p, \tag{9}$$

$$Q_3 = 2\int_{r_{2,0}}^{1} W(r)rdr = \left[\frac{1 - r_{2,0}^2}{2}\right]W_p. \tag{10}$$

Note that due to the scaling, we have $Q_1 = 1$. Figure 5 plots G_c for representative m/δ and r_1. Over the range plotted, the pressure gradient is significantly less than the pressure gradient G_o required for the heavy oil to flow alone in the pipe ($G_o = 4\pi/\frac{m}{\delta}$). Also, for small m/δ, we observe that G_c is quite independent from m/δ, as expected from (7).

The flow rate of the skin layer is given by (9) and provided that $m \ll 1$ and both the skin and lubricant layers are thin, we can expect that $W_p \approx 1$. Thus, Q_2 scales primarily with $[r_{2,0}^2 - r_1^2]$ in any lubrication regime that is effective. Figure 6 plots the intensity of the flow rate of the lubrication layer $[Q_3/(1 - r_{2,0}^2) = W_p/2]$. We observe that we are able to achieve relatively small flow rates of both the lubricant and skin fluids by varying $r_{2,0}$ and r_1. For typical heavy crude viscosity ratios

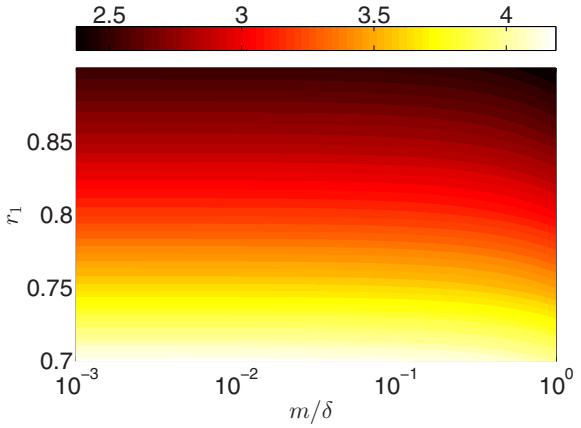

FIG. 5. Scaled pressure gradient (G_c) for representative m/δ and r_1, $r_{2,0} = 0.95$.

($m \ll 1$) the flow rate change with m is negligible both for the skin and lubricant. Finally, we show variations in the criterion (8) for different r_1 and $r_{2,0}$; see Fig. 7. We see that the minimal B increases as $r_{2,0}$ approaches the wall, as is expected.

To summarize, this simple one-dimensional (1D) model suggests that there are parameter regimes in which the triple-layer flows can provide a viable transportation method, depending of course on fluid costs and on the difficult question of establishing the triple-layer flow, in a development stage somewhere upstream. However, the concentric solution is not feasible as a core-annular flow as no lift force is generated to balance the density differences.

III. ECCENTRIC CORE-ANNULAR FLOW

Note that the concentric solution of the previous section has a pressure gradient only in the axial direction. In a typical case where the oil density differs from that of the lubricant and skin fluid, there is a net transverse buoyancy force, so that the underlying configuration is unlikely to be concentric. A uniform eccentric annular flow also generates only axial pressure gradients and, although different from the concentric considered above, cannot support density differences. As

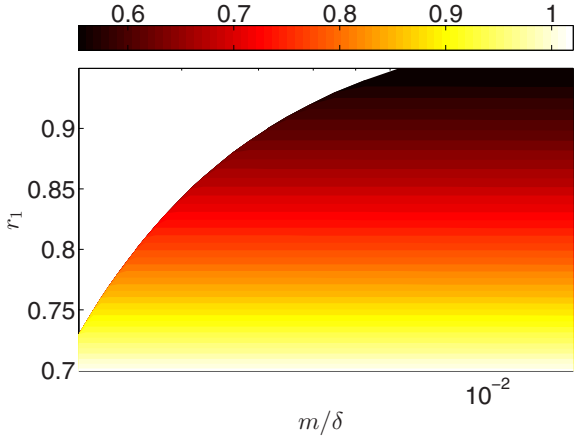

FIG. 6. Intensity of flow rate of lubricating fluid [$Q_3/(1 - r_{2,0}^2) = W_p/2$] for representative m/δ and r_1 (with $m = 0.0001$).

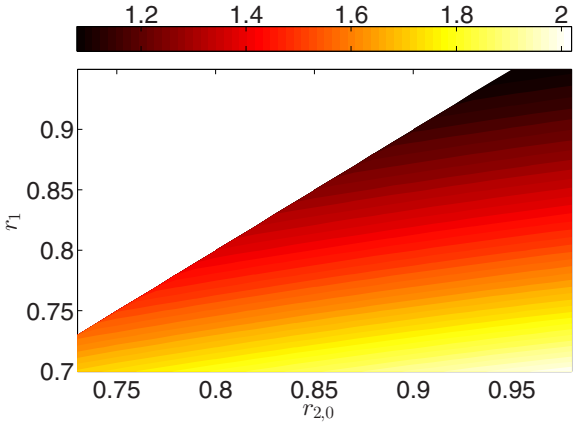

FIG. 7. Variations in the minimal B from (8), for representative $r_{2,0}$ and r_1 (with $m = 0.0001$).

recognized in Ref. [17], it is necessary to have both eccentricity and axial variation in the lubrication layer in order to generate transverse lift forces via viscous lubrication. As with any transport process, there is an underlying constant pressure drop along the pipeline. Superimposed on this is a periodic (in z) variation in the pressure, which is governed by the local thickness of the lubricant. In this way, differential lubrication pressures are generated that are able to counter the transverse buoyancy force.

Anticipating the above scenario, we use a classical lubrication scaling of the equations. As shown in Fig. 3, we position our cylindrical coordinates at the center of Ω_1, which has a uniform radius $\hat{r}_1$. The skin layer outer radius is $\hat{r}_2(\hat{z})$, which has a mean position $\hat{r}_{2,0}$ and axial variation as in Fig. 4. The pipe wall is denoted $\hat{r} = \hat{r}_3(\theta)$, with variation due to the eccentricity. We assume the mean thickness of the outer lubricant layer to be thin, relative to the circumferential and axial length scales $\pi\hat{R}$ and $\hat{l}$, respectively. In other words, $\delta = (\hat{R} - \hat{r}_{2,0})/(\pi\hat{R}) \ll 1$ and assume that $\lambda = \hat{l}/(\pi\hat{R}) \sim O(1)$. Below, we calculate the leading order in δ shear stresses and pressure in the lubricant layer. However, in typical scenarios considered, $m \ll 1$ also (even $m \lesssim \delta$), and the parameter m/δ occurs in the leading order expressions. Therefore, the practical limit we consider here is the distinguished limit $\delta \to 0$, with $m/\delta =$ finite.

Our solution below is parametrized by three dimensionless scalars: the mean frictional pressure gradient along the pipe (G), the plug velocity (W_p), and the eccentricity (e) of the core. These three scalars are determined by satisfying three integral constraints. First, the flow rate of fluid 1 has been specified in the adopted formulation,

$$\hat{Q}_1 = \hat{W}_p \pi \hat{r}_1^2 + \frac{\pi \hat{r}_1^4}{8\hat{\mu}^{[1]}}\hat{G}. \tag{11}$$

Second, the pressure drop along the pipe is balanced by the wall shear stresses,

$$0 = \int_0^{2\pi}\int_0^{\hat{r}_3} \hat{r}([-\hat{P} + \hat{\tau}_{zz}]_{\hat{z}=\hat{l}} - [-\hat{P} + \hat{\tau}_{zz}]_{\hat{z}=0})d\hat{r}d\theta + \int_0^{2\pi}\int_0^{\hat{l}} \hat{r}_3\hat{\tau}_{zr}|_{\hat{r}=\hat{r}_3} d\theta d\hat{z}. \tag{12}$$

Third, the static pressure and viscous shear forces acting on the skin in the vertical direction balance the weight of the liquid,

$$0 = (\hat{\rho}^{[3]} - \hat{\rho}^{[2]})\hat{g}\hat{V}^{[2]} + (\hat{\rho}^{[3]} - \hat{\rho}^{[1]})\hat{g}\hat{V}^{[1]} - \int_0^{2\pi}\int_0^{\hat{l}} \hat{r}_2(\hat{P}|_{\hat{r}=\hat{r}_2}\cos\theta + \hat{\tau}_{r\theta}|_{\hat{r}=\hat{r}_2}\sin\theta)d\theta d\hat{z}, \tag{13}$$

where $\hat{V}^{[1]}$ and $\hat{V}^{[2]}$ are the volume of the core and skin fluids, respectively.

The flow rate and pressure drop constraints vary linearly with the frictional pressure gradient and the plug velocity, which are easily incorporated into the solution, whereas (13) varies nonlinearly with e. To begin our analysis, we fix the eccentricity e and compute the frictional pressure gradient and plug velocity, using the flow rate and pressure drop conditions. Later in the paper we include the vertical force balance (13) to determine e.

A. Lubricating layer

We assume symmetry about a central vertical plane through the pipe, define $z = \hat{z}/\hat{l}$, define the scaled azimuthal coordinate $y = \theta/\pi$ with $y \in [0,1]$, extending from the top to the bottom of the lubricant annulus, and define x,

$$\hat{r} = \hat{r}_{2,0} + \pi \hat{R}\delta x.$$

Velocity components in the axial and azimuthal directions are scaled with $\hat{W}_0$ and that in the radial direction with $\delta \hat{W}_0$. We break the pressure into three parts: a constant axial pressure gradient, a periodic lubrication pressure (coming from the variation in layer thickness), and a hydrostatic pressure component,

$$\hat{P} = -\hat{P}_G^* G z + \hat{P}_l^* P_l(x,y,z) + \pi \delta \hat{\rho}^{[3]} \hat{g} \hat{R} x \cos(\pi y). \tag{14}$$

The lubrication pressure scale ($\hat{P}_l^*$) is chosen to balance the leading order shear stress gradients,

$$\hat{P}_l^* = \frac{\pi \hat{R} \hat{\mu}^{[3]} \hat{W}_0}{(\hat{R} - \hat{r}_{2,0})^2}. \tag{15}$$

The axial pressure gradient scale ($\hat{P}_G^*$) is similar to that is used in the concentric solution (Sec. II),

$$\hat{P}_G^* = \frac{\pi \lambda \hat{\mu}^{[3]} \hat{W}_0}{(\hat{R} - \hat{r}_{2,0})}. \tag{16}$$

Note we use $\hat{W}_0$ in the pressure scale $\hat{P}^*$ instead of the dimensional plug speed $\hat{W}_p$ because these are similar for small m, and since $\hat{W}_0$ is readily accessible. The leading order shear stresses scale with $\delta \hat{P}_l^*$.

With the above scaling, the leading order momentum equations are

$$0 = \frac{\partial P_l}{\partial x}, \tag{17}$$

$$0 = -\frac{\partial P_l}{\partial y} + \frac{\partial^2 v}{\partial x^2}, \tag{18}$$

$$0 = -\frac{1}{\lambda}\frac{\partial P_l}{\partial z} + \frac{\partial^2 w}{\partial x^2}, \tag{19}$$

$$0 = \frac{\partial u}{\partial x} + \frac{\partial v}{\partial y} + \frac{1}{\lambda}\frac{\partial w}{\partial z}. \tag{20}$$

We can see that P_l is only a function of (y,z). For the present study we assume that the skin layer moves only axially, with speed W_p to be determined. The boundary conditions for the lubricant are $(u,v,w) = (0,0,0)$ at $x = x_3(y)$ and $(u,v,w) = (0,0,W_p)$ at $x = x_2(z)$. The functions $x_3(y)$ and $x_2(z)$ are derived from the wall and outer skin positions, to leading order in δ. The thickness of the lubricant layer is denoted $h(y,z) = x_3(y) - x_2(z)$, which is given to leading order by

$$h(y,z) = 1 - e\cos\pi y - a\Phi(z) + O(\delta), \tag{21}$$

where the eccentricity is $e = \hat{d}/(\hat{R} - \hat{r}_{2,0})$ and the amplitude $a = \Delta\hat{r}_2/\pi\hat{R}\delta$. $\hat{d}$ is the radial distance between the pipe and core centers; see Fig. 3. Note that the dimensionless axial skin thickness variation $\Phi(z)$ has zero mean and maximal amplitude 1.

We treat the system (17)–(20) and boundary conditions in the usual way, eliminating the averaged (y,z)-velocity components with a stream function and then deriving the following Reynolds equation for the pressure,

$$\frac{\partial}{\partial y}\left[h^3\frac{\partial P_l}{\partial y}\right]+\frac{1}{\lambda^2}\frac{\partial}{\partial z}\left[h^3\frac{\partial P_l}{\partial z}\right]=-6\frac{W_p}{\lambda}\frac{\partial h}{\partial z}. \tag{22}$$

As we see, apart from depending on the lubrication layer geometry h, (22) is driven linearly by W_p, which is determined from the flow rate constraint and horizontal force balance. The velocity in the core fluid is easily found as a superposition of a parabolic Poiseuille profile and the plug velocity. Integrating across Ω_1, the dimensionless form of (11) is

$$1=W_p r_1^2+\frac{m}{\delta}\frac{r_1^4}{8\pi}G. \tag{23}$$

For the horizontal force balance, note that only the constant pressure gradient contributes to the pressure drop term (the other terms being periodic in z). The nondimensional version of (12) is

$$0=G+2\int_0^1\int_0^1 r_3\frac{\partial w}{\partial x}(x_3,y,z)dydz, \tag{24}$$

where $r_3=r_{2,0}+\pi\delta x_3$.

Finally, to determine the vertical displacement or eccentricity e, we scale the vertical force balance. The constant axial pressure gradient makes no contribution. To leading order in δ the balance is

$$\int_0^1\int_0^1 r_2 P_l(y,z)\cos\pi y dydz-F_l\left(1-\varrho\left[1-\frac{r_1^2}{r_{2,0}^2}\right]\right)=0. \tag{25}$$

In the above equation,

$$F_l=\frac{(\hat\rho^{[3]}-\hat\rho^{[1]})\hat g\hat R}{2\hat P_l^*}r_{2,0}^2=\delta\frac{(\hat\rho^{[3]}-\hat\rho^{[1]})\hat g\pi\hat R^2 r_{2,0}^2}{2\pi\hat R\left[\frac{\hat\mu^{[3]}\hat W_0}{(\hat R-\hat r_{2,0})}\right]},$$

which we easily identify as the ratio of buoyancy forces to lubrication pressure forces (the viscous scale amplified by δ^{-1}). The parameter ϱ arises if there is a density difference between the skin and core fluids,

$$\varrho=\frac{\hat\rho^{[1]}-\hat\rho^{[2]}}{\hat\rho^{[3]}-\hat\rho^{[1]}}.$$

For simplicity, we shall assume that $\varrho=0$ in this study, so that F_l must balance with the lubrication force generated through P_l.

B. Solution method

Note that the Reynolds equation describes flow in a symmetric geometry $h(y,z)$ and we thus seek a symmetric solution by imposing symmetry conditions at $y=0$ and $y=1$, together with periodicity in z. As the lubricant is Newtonian, (22) is linear and is symmetric due to $h(y,z)$. Consequently, we may find the solution as $P_l=W_pP_l^{[0]}$, driven by plug velocity W_p. For fixed geometry the solution $P_l^{[0]}$ corresponds to the pressure fields generated at the unit plug velocity. To find $P_l^{[0]}$ we have used a second-order central finite difference approximation to discretize (22) and then solve the linear algebraic system with MATLAB.

Substitution of the velocity into (24) leads to

$$G=2\int_0^1\int_0^1\left[\frac{W_p}{h}-\frac{h}{2\lambda}\left(\frac{\partial P_l}{\partial z}\right)\right]dydz \tag{26}$$

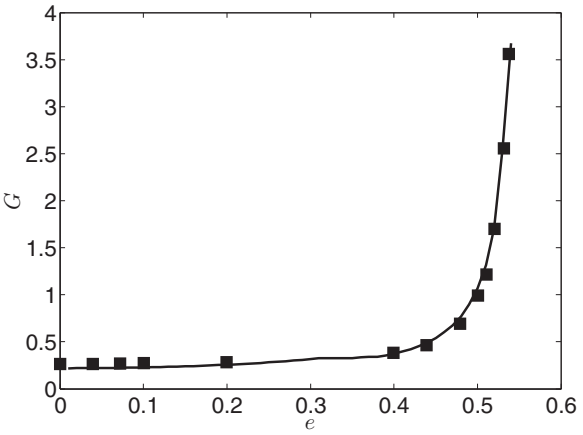

FIG. 8. Axial pressure gradient for the current study (solid line) and from Ooms *et al.* [15].

$[r_3 \sim 1 + O(\delta)]$, and G is eliminated by

$$G = \left(1 - W_p r_1^2\right) \frac{8\pi}{r_1^4} \frac{\delta}{m}. \tag{27}$$

Now, W_p can be found by solving (26) and (27) simultaneously,

$$W_p = \frac{\frac{1}{r_1^2}}{1 + \frac{m}{\delta} \frac{r_1^2}{4\pi} \int_0^1 \int_0^1 \left[\frac{1}{h} - \frac{h}{2\lambda} \frac{\partial P_l^{[0]}}{\partial z}\right] dy dz}. \tag{28}$$

We verify the solution by comparison with that of Ooms *et al.* [15], who consider a two-layer eccentric core-annular flow with a wavy profile in the axial direction and infinite relative viscosity between the core and lubricant. Figure 8 shows the comparison of the axial pressure gradient. The results match well, with the very small discrepancy attributable to a numerical error. In Ref. [15] the core viscosity is infinite so it has rigid body motion and the core wall is wavy. A second comparison is shown in Fig. 9, this time comparing the pressure variations between the current model and the

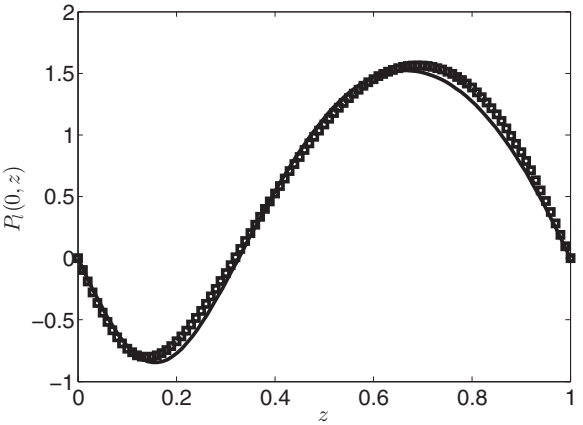

FIG. 9. Periodic pressure variation along z for the current study (solid line) and from Ooms *et al.* [17].

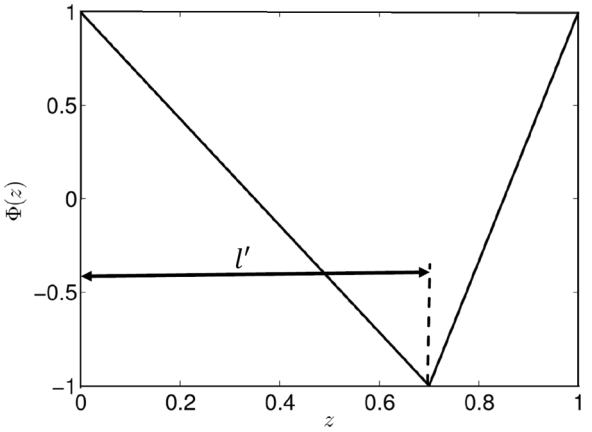

FIG. 10. Sawtooth outer skin profile $\Phi(z)$.

results of Ref. [17]. The small differences are probably because of different solution methods: Ooms *et al.* use an asymptotic approximation to solve the Reynolds equation.

IV. RESULTS

For all the results below, we assume a sawtooth profile for the skin shape function $\Phi(z)$, as illustrated in Fig. 10. The parameter l' is referred to as the *break point* of the wave. This configuration is chosen as it is relatively simple and the asymmetry in z is necessary to generate lubrication pressures that can support the buoyancy forces of the core and skin fluids; see Ref. [17].

A. Example flow

The flows are parametrized by six dimensionless parameters $(r_1, e, m/\delta, l', \lambda, a)$ if e is specified and F_l calculated. Alternatively, F_l may be specified and e calculated. We discuss typical parameters in more detail and explore the parametric variations below in Sec. IV B. As an illustration of an example flow, we solve with $(r_1, e, m/\delta, l', \lambda, a) = (0.87, 0.6, 0.1, 0.7, 1, 0.3)$, assuming a sufficiently large Bingham number to prevent yielding of the skin. Here, e is set relatively large, to emphasize eccentricity effects.

The lubrication layer thickness and associated periodic pressure are indicated in Fig. 11, at different azimuthal positions y. As expected, it can be seen that for the narrower gaps (near the top of the pipe) the amplitude of the pressure variation increases, generating significant pressures within the lubricant. In this case we have $l' = 0.7$, which results in a net upwards lubrication force (that might be used to balance buoyancy in a case where the core fluids are heavier that the lubricant). Note that in general we would have $l' < 0.5$ to generate a net downwards force.

Figure 12 shows the variation of the layer-averaged velocity in the lubrication layer. Here, we have *unwrapped* the annulus into the (y, z) plane. We observe a small secondary azimuthal flow relative to the main axial flow, i.e., the fluid is squeezed in and out of the narrower parts of the annulus near the top of the pipe ($y = 0$).

B. Parametric variations

To develop intuition about the effect of the geometric parameters and fluid properties on the main process variables (G, Q_2, Q_3, F_l), we now systematically explore variations over representative ranges of variables. The dimensional parameters relevant to these flows are extracted from the literature and summarized in Table I; see, e.g., Refs. [22–29] and many others. Based on Table I, we can find the ranges over which the nondimensional numbers typically vary (see Table II).

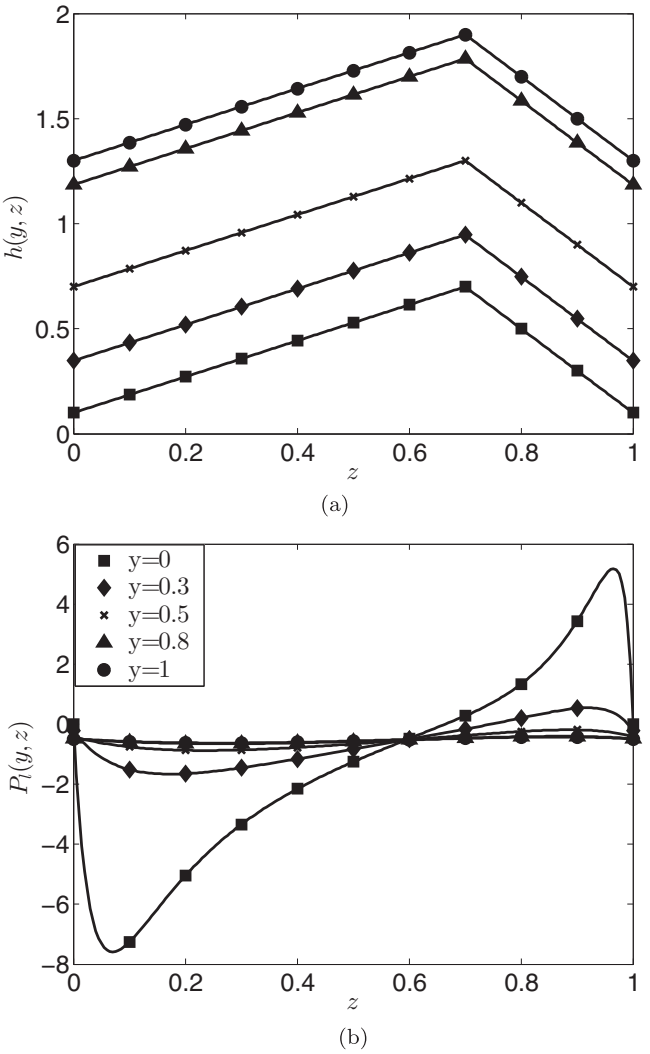

FIG. 11. Variations with z at fixed y. (a) lubricant layer thickness $h(y,z)$ and (b) lubrication pressure $P_l(y,z)$.

In terms of our study and the proposed method, the variables r_1 and $r_{2,0}$ should remain close to 1 to minimize consumption of the lubricant and skin fluids. This is essentially an economic constraint: Typical lubricant fractions used vary in the range 5%–20%. Although $\delta \ll 1$, typically also $m < \delta$ and to some extent one could vary $m/\delta < 1$ in designing the flow. The wave form $\Phi(z)$ should be regarded as being designable, i.e., amplitude a, *break point* l', and wavelength λ. However, we might expect $\lambda = O(1)$ and note that $a + e < 1$ to avoid contact. The eccentricity e will eventually be determined below to balance the lubrication force.

1. Varying skin profile

Here, we fix a moderate eccentricity and explore the effects of wave shape on the flow, for $(r_1,e,m/\delta,\lambda) = (0.87,0.3,0.1,1)$. The wave shape $\Phi(z)$ is governed by its amplitude (a), the break point of the wave (l'), and its wavelength (λ). Figure 13 shows the normalized pressure gradient required, G/G_o. It can be seen that the effect of l' is negligible, whereas increasing a

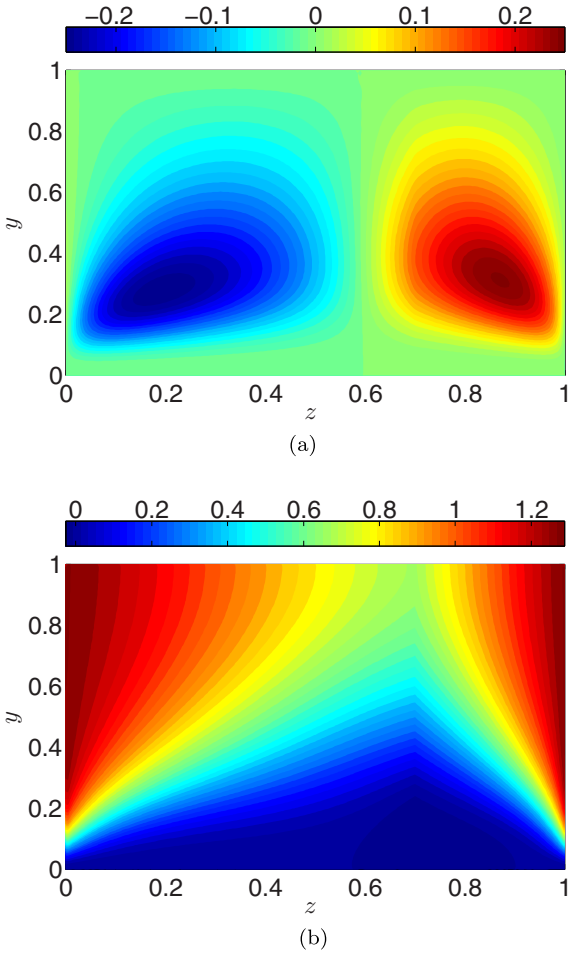

FIG. 12. Layer-averaged velocity in the lubricant layer, for the same parameters as in Fig. 11. (a) Layer-averaged azimuthal velocity and (b) Layer-averaged axial velocity.

significantly decreases the pressure gradient. This arises because the pressure gradient is determined disproportionately by the narrowest parts of the lubrication layer.

The required flow rate of the lubricating fluid (Q_3) is presented in Fig. 14. As with the pressure gradient (Fig. 13), the variation of the flow rate does not change significantly with l'. It seems that Q_3 increases as a increases. This may seem at odds with the pressure gradient variation in Fig. 13, which decreases. Note, however, that the flow rate of the lubricating layer includes two components: a pressure driven flow rate and plug velocity flow rate, say, Q_{3,W_p}. The inset of Fig. 14 shows Q_3

TABLE I. Dimensional parameter ranges found in heavy crude oil pipelining.

Variable	Symbol	Range
Crude oil viscosity	$\hat{\mu}^{[1]}$	0.1–100 Pa s
Crude oil density	$\hat{\rho}^{[1]}$	770–980 kg/m^3
Pipe radius	$\hat{R}$	0.05–0.61 m
Crude oil velocity	$\hat{W}_0$	0.5–5 m/s

TABLE II. Ranges of key dimensionless numbers expected in typical pipelining operations.

Dimensionless number	Symbol	Range
Aspect ratio	δ	0.01–0.03
Viscosity ratio	m	0.000 01–0.01
Density ratio	$\hat{\rho}^{[3]}/\hat{\rho}^{[1]}$	1.02–1.3
Buoyancy to lubrication force ratio	F_l	0.014–2

and Q_{3,W_p}. The latter is the dominant contribution to Q_3 and increases with a: The pressure driven component decreases (see the difference between the two curves in the inset). Variations in Q_2 are not shown, but are negligible.

The effect of l' thus far seems insignificant, but this only considers (G, Q_2, Q_3). If instead we compute the leading order net lubrication force from (25), i.e.,

$$\int_0^1 \int_0^1 P_l(y,z)\cos\pi y dy dz,$$

this gives the value of the dimensionless F_l that can be supported. As we recall, F_l represents the dimensionless ratio of buoyancy force to the scaling for the net lubrication force. Figure 15 plots the variation of the net lubrication force with l' and a. The main point to note is that the net lubrication force changes sign along a critical curve, say, $a_c(l')$. In a balanced system, satisfying (25), this figure shows F_l. Thus for a significant positive F_l, in this example we need $l' < 0.45$ and a sufficiently large a. In this example, we have fixed the eccentricity at a modest $e = 0.3$, and the supported F_l is modest. As we have remarked in the previous section, $F_l < 0$ is generated for $l' > 0.5$. Although we can support a denser core fluid in this way, note that, practically speaking, the eccentricity would no longer be positive.

We now explore the effects of the wavelength (λ). The normalized pressure gradient (G/G_o) is shown in Fig. 16. Although there is a modest variation with a, λ has an insignificant effect on the pressure drop. Similarly, the effect of λ on the flow rates Q_2 and Q_3 is found to be negligible. Figure 17 shows the effect of λ on the computed net lubrication force. Although there is a variation, it is not significant.

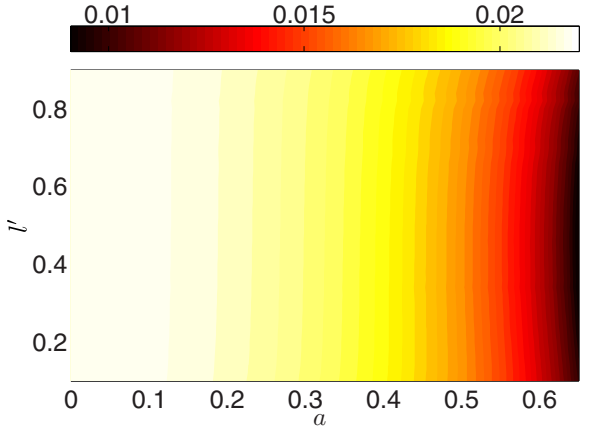

FIG. 13. Normalized pressure gradient (G/G_o) for different a and l'; fixed parameters $(r_1, e, m/\delta, \lambda) = (0.87, 0.3, 0.1, 1)$.

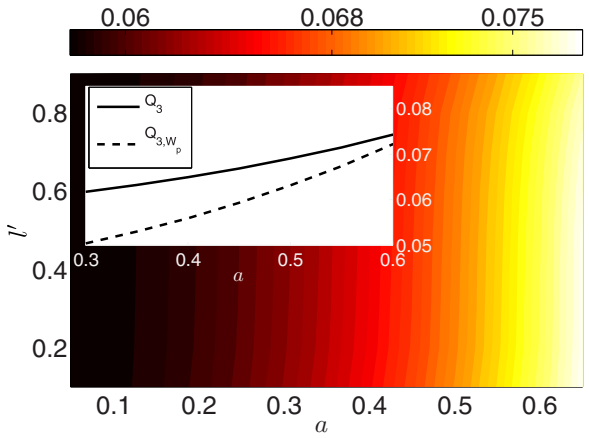

FIG. 14. Flow rate of lubricating fluid (Q_3) for different a and l'; fixed parameters $(r_1,e,m/\delta,\lambda) = (0.87,0.3,0.1,1)$. The inset shows the total flow rate and partial flow rate due to W_p of the lubricating layer when $l' = 0.2$.

In conclusion, we fix $(\lambda,l') = (1,0.2)$ for the remainder of the study: Varying λ has little effect and l' in this range ensures a buoyancy balance for positive e. The amplitude a remains as a control parameter, but is also limited by e.

2. Varying viscosity ratio and geometry

We now study variations in $(r_1,m/\delta)$. We first fix $(e,l',\lambda,a) = (0.3,0.2,1,0.5)$ and vary $(r_1,m/\delta)$ within admissible ranges. Figure 18 shows the variation of the normalized pressure gradient G/G_o. As expected, this increases with m/δ, and also decreases with r_1. To aid visualization, we have superimposed the contour $G/G_o = 0.1$, and see that even for $m/\delta \approx 0.7$ we have a pressure gradient of less than 10% of the crude oil pressure gradient (and indeed normally we would expect to be far below that). Note, however, that this is with a relatively thin lubricating layer.

Regarding the flow rates, the scaled skin fluid flow rate is $W_p(r_{2,0}^2 - r_1^2)$. As discussed previously, variations in W_p are small for small m/δ. Figure 19 plots the flow rate of the lubricant (Q_3), which is

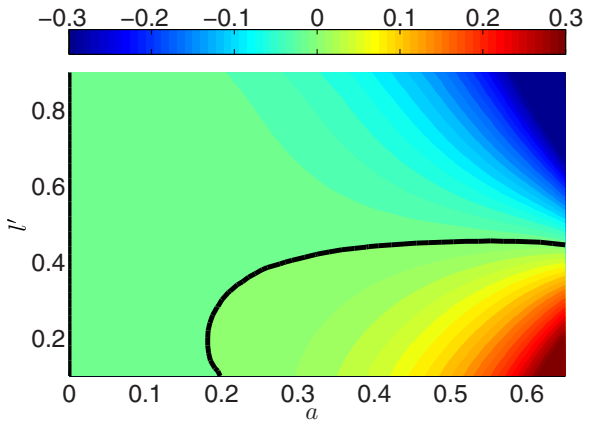

FIG. 15. Computed net lubrication force able to balance F_l for different a and l'; fixed parameters $(r_1,e,m/\delta,\lambda) = (0.87,0.3,0.1,1)$. The solid black line is where no density difference can be supported ($F_l = 0$).

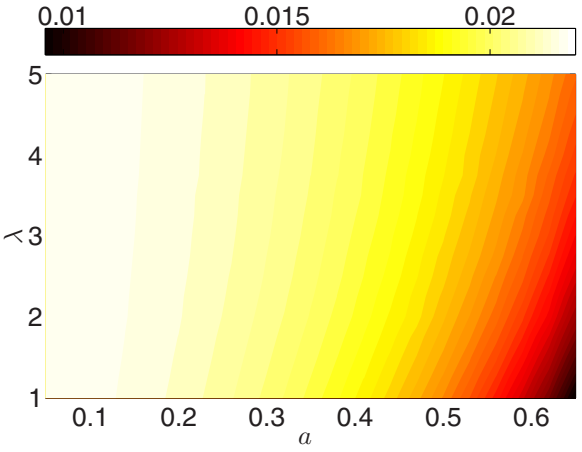

FIG. 16. Normalized pressure gradient (G/G_o) for different a and λ; fixed parameters $(r_1,e,m/\delta,l') = (0.87,0.3,0.1,0.2)$.

practically invariant with small m/δ, but decreases with r_1 for larger $m/\delta \lessapprox 1$. Thus, to acceptably control G/G_o, we adjust m/δ, either via m or $r_{2,0}$ (δ). The flow rates (consumption) of the skin and lubricant fluids may then be partially controlled by varying r_1.

The computed net lubrication force that is able to balance F_l is shown for the same parameters in Fig. 20. It can be seen that m/δ has a relatively small effect on the lubrication force, which varies mostly with r_1. Having said this, the variations here are relatively modest due to the small eccentricity e.

The final geometric parameter is the eccentricity e. The flow rates are not significantly affected by e, so we focus on the pressure gradient and lubrication force. Figure 21 shows the scaled pressure gradient for different eccentricities and core radii, where $(m/\delta,l',\lambda,a) = (0.1,0.2,1,0.5)$. We can see the pressure gradient mostly varies with r_1, except when $e + a \approx 1$, where we see a significant

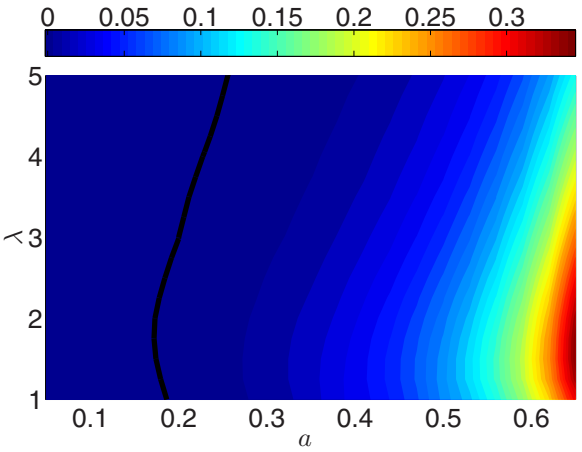

FIG. 17. Computed net lubrication force able to balance F_l for different a and λ; fixed parameters $(r_1,e,m/\delta,l') = (0.87,0.3,0.1,0.2)$. The solid black line is where no density difference can be supported $(F_l = 0)$.

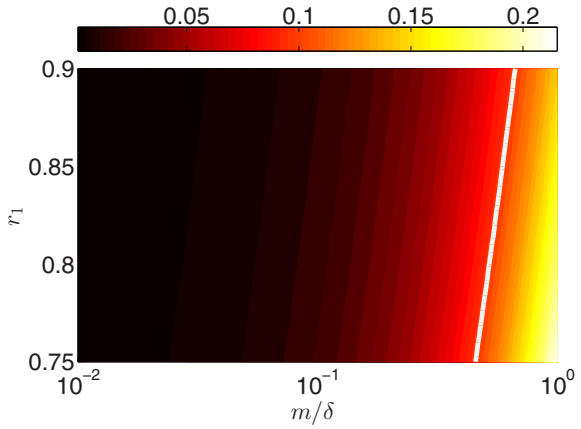

FIG. 18. Normalized pressure gradient (G/G_o) for different m/δ and r_1; fixed parameters $(e,l',\lambda,a) = (0.3,0.2,1,0.5)$. The solid white contour marks $G/G_o = 0.1$.

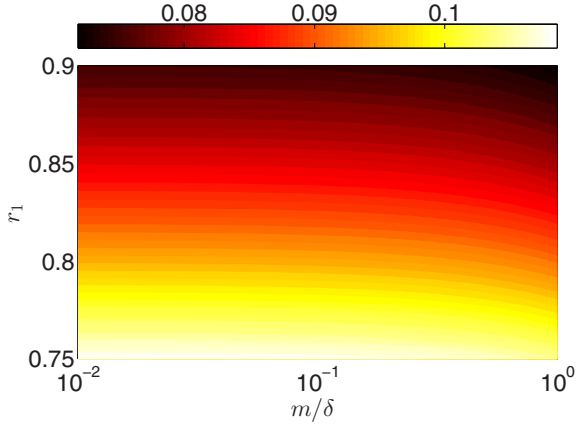

FIG. 19. Flow rate of lubricating fluid (Q_3) for different m/δ and r_1; fixed parameters $(e,l',\lambda,a) = (0.3,0.2,1,0.5)$.

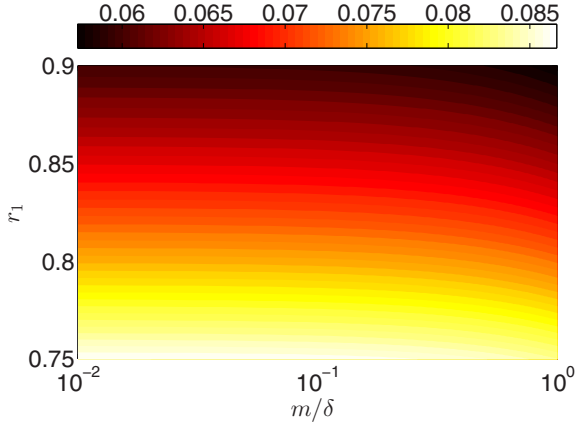

FIG. 20. Computed net lubrication force able to balance F_l for different m/δ and r_1; fixed parameters $(e,l',\lambda,a) = (0.3,0.2,1,0.5)$.

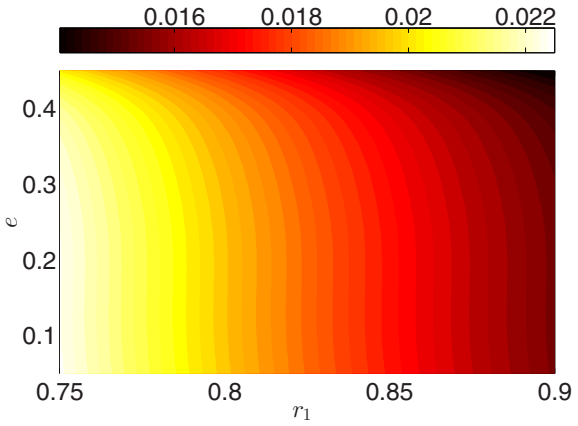

FIG. 21. Normalized pressure gradient (G/G_o) for different r_1 and e; fixed parameters $(m/\delta,l',\lambda,a) = (0.1,0.2,1,0.5)$.

decrease with e. Thus, in total we see that varying e does not have any detrimental effect on the pressure gradient.

The net lubrication force which is able to balance the density difference is shown in Fig. 22 for different r_1 and e. Here, by contrast, we see that the net lubrication force varies strongly with e and weakly with r_1. As might be expected, more eccentric flow configurations are able to support larger density differences with the core fluid. The mechanism is straightforward: The lubricant layer at the top of the pipe thins and contributes larger pressures to the net lubrication force.

C. Balance position

In general, for fixed $(r_1,m/\delta,l',\lambda,a)$, as we increase the eccentricity, the net lubrication force increases; see Fig. 22, for example. Eventually, according to the value of a, the skin contacts the wall, which is to be avoided. However, before this eccentricity is attained, a certain range of F_l can be supported.

For a fixed specified F_l we iteratively solve (25) for e. For fixed $(r_1,m/\delta,l',\lambda,a)$, Eq. (25) appears to be a monotonically increasing function of e, with a single root that represents the balance eccentricity.

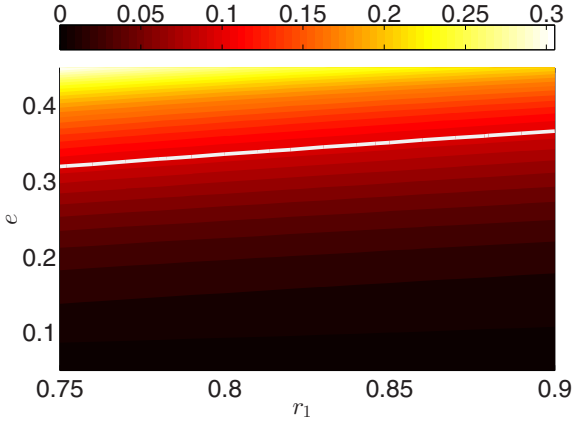

FIG. 22. Computed net lubrication force able to balance F_l for different r_1 and e; fixed parameters $(m/\delta,l',\lambda,a) = (0.1,0.2,1,0.5)$. The solid white line shows $F_l = 0.1$.

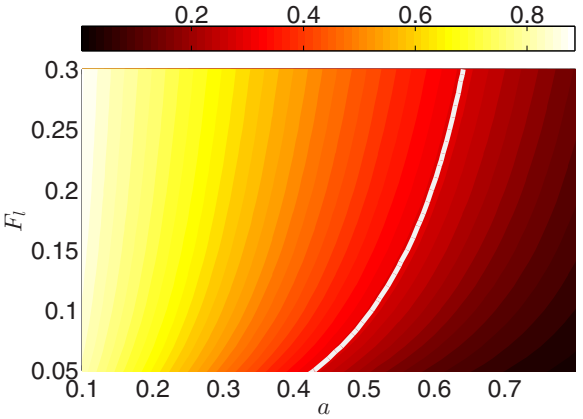

FIG. 23. Variation of the eccentricity (e) required to balance F_l, for different a and F_l. Fixed parameters are $(m/\delta, l', \lambda, r_1) = (0.1, 0.2, 1, 0.87)$. The solid white line is a guide to the eye, showing $e = 0.3$.

This is straightforwardly found using a bisection method. Figure 23 shows the eccentricity needed to generate buoyancy forces for different values of F_l. It should be noted that in this figure at each F_l, e is adjusting with respect to a to ensure a sufficiently narrow gap on the top of the pipe, i.e., the narrowest gap is $h(y,z) = h_{\min} = 1 - e - a$, and it is in the vicinity of the narrowest gap that we generate the largest lubrication pressures. However, there is in fact a significant variation in $h_{\min}$ as (a, F_l) vary, as illustrated in Fig. 24, i.e., a combination of a and e results in the distribution of $h(y,z)$ about $h_{\min}$. As we see, the largest $h_{\min}$ appear to arise in the range $a \approx 0.55$–0.65 for these parameters and, as we expected, for smaller F_l, $h_{\min}$ is larger.

The relative pressure gradient is presented in Fig. 25 for different a and F_l. The larger values of a give rise to smaller equilibrium e and reduced frictional pressures. However, in all cases (even though $m/\delta = 0.1$), the relative pressure gradient is relatively small.

The flow rate of the skin fluid is largely unaffected by the balance position of the core fluid (i.e., finding e). As expected, it varies with the wave amplitude and as the skin layer gets narrower, the flow rate of the skin fluid decreases. The flow rate of the lubricant is shown in Fig. 26. The required flow rate increases when the wave amplitude a increases.

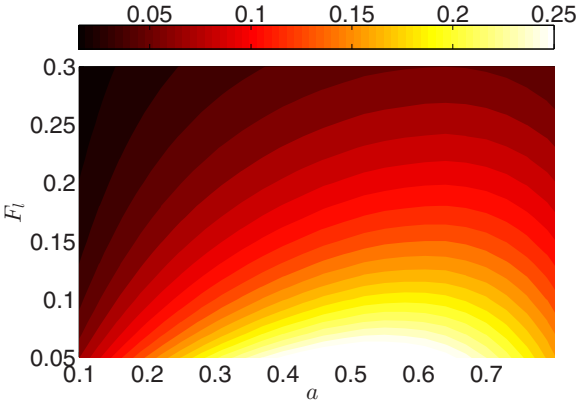

FIG. 24. Variation of the minimal layer thickness $h_{\min} = 1 - e - a$ for the balance eccentricity. Fixed parameters are $(m/\delta, l', \lambda, r_1) = (0.1, 0.2, 1, 0.87)$.

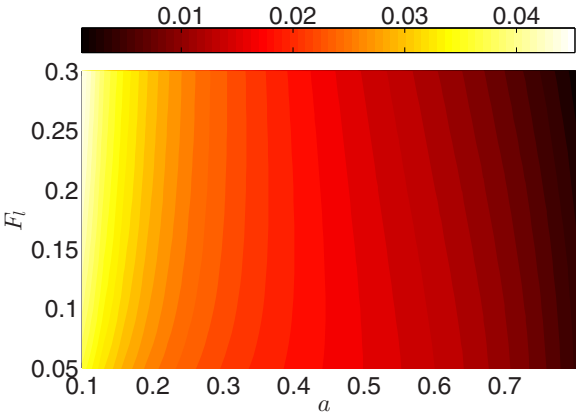

FIG. 25. Normalized pressure gradient (G/G_o) in the balance state, for different a and F_l; fixed parameters $(m/\delta,l',\lambda,r_1) = (0.1,0.2,1,0.87)$.

D. Estimating the minimal yield stress in the skin

The final important design parameter is the yield stress required to keep the skin layer completely unyielded. In practice, the stresses generated in the lubrication layer are quite localized. As an illustration, for $(m/\delta,l',\lambda) = (0.1,0.2,1)$, we fix $(a,r_1,F_l) = (0.5,0.87,0.1)$ and compute the equilibrium eccentricity $e = 0.313\,585\,8$. For this solution we plot the shear stress at the interface with the skin layer $(r = r_2)$ in Fig. 27. The shear stress is continuous at the interface and therefore this represents one measure of the deviatoric stresses within the skin layer. We can see that this is not extreme.

Second, if we consider the x-momentum equation in the skin layer,

$$\frac{\partial \tau_{xy}^{[2]}}{\partial y} + \frac{1}{\lambda}\frac{\partial \tau_{xz}^{[2]}}{\partial z} = \frac{\partial P}{\partial x} + O(\delta^2), \tag{29}$$

we see that the shear stresses in the skin also adjust to accommodate normal stress gradients. The axial pressure gradient $-Gz$ transmits across the skin, driving the flow. The lubrication pressure,

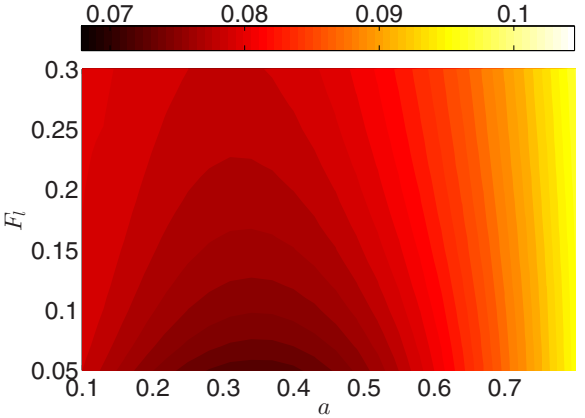

FIG. 26. Flow rate of lubricating fluid (Q_3) in a balance state, for different a and F_l; fixed parameters $(m/\delta,l',\lambda,r_1) = (0.1,0.2,1,0.87)$.

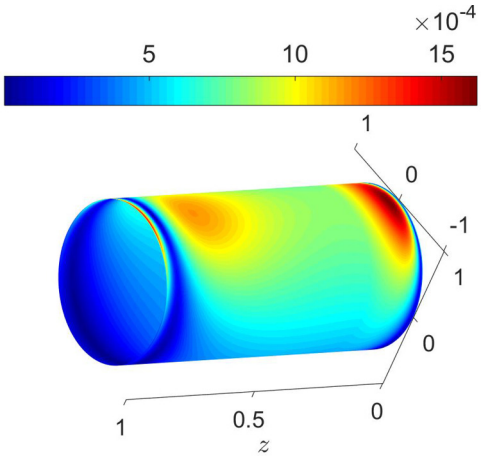

FIG. 27. Shear stress at $r = r_2$, for $(m/\delta, l', \lambda, a, r_1, e) = (0.1, 0.2, 1, 0.5, 0.87, 0.3136)$.

however, vanishes on the inner radius $r = r_1$. Therefore, we estimate

$$\frac{\partial P}{\partial x} \approx \frac{P_l}{x_2 - x_1}$$

for the right-hand side of (29). We then integrate the shear stressed throughout the skin, in (y, z), to give a rough estimate for $\tau^{[2]}$,

$$\tau^{[2]} \approx \frac{|P_l|}{x_2 - x_1}.$$

The normal stresses are typically one order larger than the shear stresses in lubrication problems and here we again amplify by insisting that the normal stresses vanish at $r = r_1$. Thus, the above estimate is generally much larger than that based on the shear stresses alone. Figure 28 shows the variation in $|P_l|/(x_2 - x_1)$ for the same parameters as in Fig. 27. The maximum normal stress is in the narrowest part of the lubricating layer, but this is modulated slightly by having larger $x_2 - x_1$. The stresses are clearly much larger than in Fig. 27.

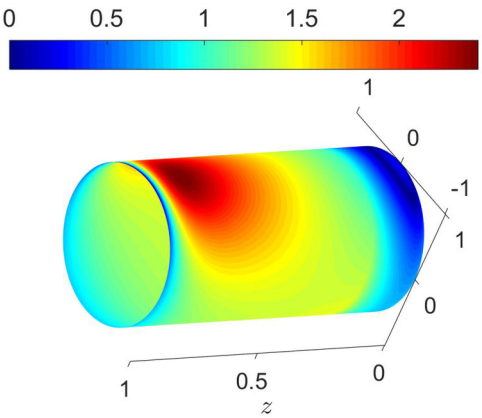

FIG. 28. Variation of $|P_l|/(x_2 - x_1)$, for $(m/\delta, l', \lambda, a, r_1, e) = (0.1, 0.2, 1, 0.5, 0.87, 0.3136)$.

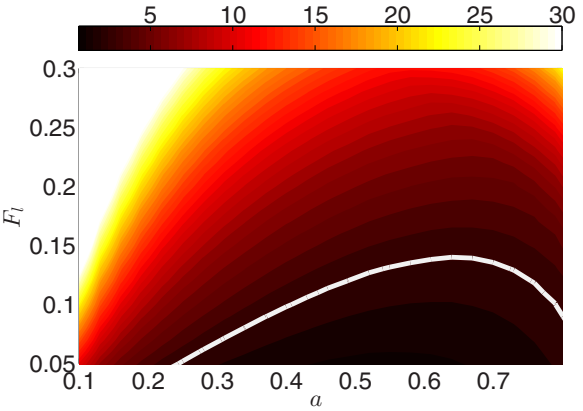

FIG. 29. Computed minimal dimensionless yield stress $B_{\min}$ needed to keep the skin layer completely unyielded in a balance state, for different a and F_l; fixed parameters $(m/\delta,l',\lambda,r_1) = (0.1,0.2,1,0.87)$. The solid white contour marks $B_{\min} = \pi$.

Now we simply consider as an estimate of the shear stress the maximum of $|P_l|/(x_2 - x_1)$, i.e., we require the minimal yield stress to satisfy

$$B > B_{\min} = \max_{(y,z)} \left(\frac{|P_l|}{x_2 - x_1} \right). \tag{30}$$

We believe that this should give a reasonable estimate of the maximal skin shear stresses, which we note are generally indeterminate for a yield stress fluid. To summarize, for fixed $(m/\delta,l',\lambda,a,r_1,F_l)$, we first compute the equilibrium value of e, and then the minimal $B_{\min}$ from (30). Figure 29 plots $B_{\min}$ for the same parameters as in the previous section. It can be seen that $B_{\min}$ is $O(1)$ and adopts moderate values within a wide range of (a,F_l).

V. DISCUSSION

We have developed a lubrication model of a three-layer lubrication flow aimed at heavy-oil transport. We have then systematically explored the parametric variations of the solutions, with the aim of establishing the feasibility of this methodology.

An attractive feature of our results is that many dimensionless parameter variations do not appear to cause significant variations in the critical parameters (G,Q_2,Q_3) that would be considered as process costs. For example, (λ,l') have a very limited effect, and m/δ affects primarily G. The flow rates of the skin and lubricant are only marginally affected by any parameters other than r_1, a, and $r_{2,0}$, but anyway remain within ranges that are economic compared to current practices in lubricated pipelining.

The feasibility therefore rests with the range of F_l that is supported. Although we may find $F_l \approx 2$, these relate to larger pipelines and larger density differences. A great many situations are covered by $F_l \lessapprox 0.3$, as explored above. Note also that smaller F_l are straightforwardly accommodated with smaller e. Nevertheless, we consider our methodology to be targeted at modest diameter pipelines.

To recover the meaning of F_l, we simply insert dimensional parameters into the definition of F_l,

$$F_l = \frac{\pi\delta^2}{2m} \frac{(\hat{\rho}^{[3]} - \hat{\rho}^{[1]})\hat{g}\hat{r}_{2,0}^2}{\hat{\mu}^{[1]}\hat{W}_0}.$$

For example, if a $150\,\mathrm{kg/m^3}$ density difference needs to be supported for a geometrical configuration, $(r_1,m/\delta,l',\lambda) = (0.87,0.1,0.2,1)$, we find $F_l \approx 0.1$ for $(m,\hat{R},\hat{W}_0,\hat{\mu}^{[1]}) =$

(0.005, 0.1 m, 1 m/s, 10 Pa s). For these same parameters the solid white contour in Fig. 29 corresponds to a yield stress of $\hat{\tau}_y^{[2]} \approx 10$ Pa.

Yield stress values in the range 1–10^2 Pa are easily found in polymer gels, even at relatively low concentrations, and/or in various emulsions. Therefore, it would appear that the design of a suitable skin system is feasible, e.g., using an emulsion of the transported oil and water. For extreme viscosities of oil, using viscosified lubricants (i.e., relative to water) can still provide a reasonable reduction of G/G_o while allowing for a designed variation of m/δ. Decreasing the density of the lubricant is less practical if water-based fluids are used.

In conclusion, it appears that the proposed method is suitable for stable lubricated pipelining of a range of heavy crude oils in moderately sized pipelines, e.g., $\hat{R} \lessapprox 20$ cm. The next steps in this research will focus on the stability of the steady flows derived here and the development lengths needed to attain the balance position.

ACKNOWLEDGMENTS

We greatly appreciate the financial support of the Natural Sciences and Engineering Research Council of Canada via their Discovery Grants programme (Grant No. RGPIN-2015-06398)

[1] M. E. Charles, G. W. Govier, and G. W. Hodgson, The horizontal pipeline flow of equal density oil-water mixtures, Can. J. Chem. Eng. **39**, 27 (1961).

[2] R. V. A. Oliemans and G. Ooms, Core-Annular Flow of Oil and Water through a Pipeline, in *Multiphase Science and Technology*, edited by G. F. Hewitt, J. M. Delhaye, and N. Zuber (Springer, Berlin, 1986), Vol. 2, p. 427.

[3] D. D. Joseph and Y. Y. Renardy, *Fundamentals of Two-Fluid Dynamics, Part II: Lubricated Transport, Drops and Miscible Liquids* (Springer, New York, 1993).

[4] D. D. Joseph, R. Bai, K. P. Chen, and Y. Y. Renardy, Core-annular flows, Annu. Rev. Fluid Mech. **29**, 65 (1997).

[5] K. C. Sahu, Double-diffusive instability in core-annular pipe flow, J. Fluid Mech. **789**, 830 (2016).

[6] M. A. Moyers-Gonzalez, I. A. Frigaard, and C. Nouar, Nonlinear stability of a visco-plastically lubricated viscous shear flow, J. Fluid Mech. **506**, 117 (2004).

[7] S. Hormozi, K. Wielage-Burchard, and I. A. Frigaard, Entry, start up and stability effects in visco-plastically lubricated pipe flows, J. Fluid Mech. **673**, 432 (2011).

[8] I. A. Frigaard, Super-stable parallel flows of multiple visco-plastic fluids, J. Non-Newtonian Fluid Mech. **100**, 49 (2001).

[9] C. K. Huen, I. A. Frigaard, and D. M. Martinez, Experimental studies of multi-layer flows using a visco-plastic lubricant, J. Non-Newtonian Fluid Mech. **142**, 150 (2007).

[10] S. Hormozi, K. Wielage-Burchard, and I. A. Frigaard, Multi-layer channel flows with yield stress fluids, J. Non-Newtonian Fluid Mech. **166**, 262 (2011).

[11] S. Hormozi and I. A. Frigaard, Nonlinear stability of a visco-plastically lubricated viscoelastic fluid flow, J. Non-Newtonian Fluid Mech. **169-170**, 61 (2012).

[12] K. C. Sahu, P. Valluri, P. D. M. Spelt, and O. K. Matar, Linear instability of pressure-driven channel flow of a Newtonian and a Herschel-Bulkley fluid, Phys. Fluids **19**, 122101 (2007).

[13] K. C. Sahu and O. K. Matar, Three-dimensional linear instability in pressure-driven two-layer channel flow of a Newtonian and a Herschel-Bulkley fluid, Phys. Fluids **22**, 112103 (2010).

[14] G. Ooms and H. L. Beckers, The flow of a rigid core surrounded by an annular liquid layer through a horizontal tube, Appl. Sci. Res. **26**, 321 (1972).

[15] G. Ooms, A. Segal, A. J. van der Wees, R. Meerhoff, and R. V. A. Oliemans, A theoretical model for core-annular flow of a very viscous oil core and a water annulus through a horizontal pipe, Int. J. Multiphase Flow **10**, 41 (1983).

[16] R. Bai, K. Chen, and D. D. Joseph, Lubricated pipelining: Stability of core-annular flow. Part 5. Experiments and comparison with theory, J. Fluid Mech. **240**, 97 (1992).
[17] G. Ooms, M. J. B. M. Pourquie, and J. C. Beerens, On the levitation force in horizontal core-annular flow with a large viscosity ratio and small density ratio, Phys. Fluids **25**, 032102 (2013).
[18] G. Ooms and P. Poesio, Analytical study of slightly eccentric core-annular flow, J. Eng. Math. **85**, 65 (2014).
[19] S. Hormozi, D. M. Martinez, and I. A. Frigaard, Stable core-annular flows of viscoelastic fluids using the visco-plastic lubrication technique, J. Non-Newtonian Fluid Mech. **166**, 1356 (2011).
[20] S. Hormozi, G. Dunbrack, and I. A. Frigaard, Visco-plastic sculpting, Phys. Fluids **26**, 093101 (2014).
[21] A. Maleki, S. Hormozi, A. Roustaei, and I. A. Frigaard, Macro-size drop encapsulation, J. Fluid Mech. **769**, 482 (2015).
[22] R. G. Santos, W. Loh, A. C. Bannwart, and O. V. Trevisan, An overview of heavy oil properties and its recovery and transportation methods, Braz. J. Chem. Eng. **31**, 571 (2014).
[23] R. Martnez-Palou, M. de Lourdes Mosqueira, B. Zapata-Rendn, E. Mar-Jurez, C. Bernal-Huicochea, J. de la Cruz Clavel-Lpez, and J. Aburto, Transportation of heavy and extra-heavy crude oil by pipeline: A review, J. Pet. Sci. Eng. **75**, 274 (2011).
[24] B. P. Hollebone, Appendix A: The Oil Properties Data Appendix, in *Handbook of Oil Spill Science and Technology* (Wiley, Hoboken, NJ, 2014), p. 575.
[25] Environment Canada ETC Spills Technology Databases, Oil Properties Database, http://www.etc-cte.ec.gc.ca/databases/oilproperties/, accessed: 2016-08-23.
[26] National Academies of Sciences, Engineering, and Medicine, *Spills of Diluted Bitumen from Pipelines: A Comparative Study of Environmental Fate, Effects, and Response* (The National Academies Press, Washington, DC, 2016).
[27] J. L. Kennedy, *Oil and Gas Pipeline Fundamentals* (PennWell, Tulsa, OK, 1993).
[28] R. Miesen, G. Beijnon, P. E. M. Duijvestijn, R. V. A. Oliemans, and T. Verheggen, Interfacial waves in core-annular flow, J. Fluid Mech. **238**, 97 (1992).
[29] P. A. M. Boomkamp and R. H. M. Miesen, Nonaxisymmetric waves in core-annular flow with a small viscosity ratio, Phys. Fluids A **4**, 1627 (1992).